Does Knowing the Oceanic PDO Phase Help Predict the Atmospheric Anomalies in Subsequent Months?

ARUN KUMAR

Climate Prediction Center, NOAA/NWS/NCEP, College Park, Maryland

HUI WANG

Climate Prediction Center, NOAA/NWS/NCEP, College Park, Maryland, and Wyle Science, Technology, and Engineering Group, McLean, Virginia

WANQIU WANG, YAN XUE, AND ZENG-ZHEN HU

Climate Prediction Center, NOAA/NWS/NCEP, College Park, Maryland

(Manuscript received 21 January 2012, in final form 4 October 2012)

ABSTRACT

Based on analysis of a coupled model simulations with and without variability associated with the El Niño–Southern Oscillation (ENSO), it is demonstrated that knowing the current value of the ocean surface temperature–based index of the Pacific decadal oscillation (the OPDO index), and the corresponding atmospheric teleconnection pattern, does not add a predictive value for atmospheric anomalies in subsequent months. This is because although the OPDO index evolves on a slow time scale, it does not constrain the atmospheric variability in subsequent months, which retains its character of white noise stochastic variability and remains largely unpredictable. Further, the OPDO adds little to the atmospheric predictability originating from the tropical Pacific during ENSO years.

1. Introduction

Previous analyses have documented atmospheric and terrestrial influences of the Pacific decadal oscillation (PDO; in this paper by PDO we mean the PDO index based on the ocean surface temperature variability in North Pacific, and henceforth, will be referred to as the OPDO index). Examples of analyses include developing El Niño–Southern Oscillation (ENSO) composites conditional to different phases of the OPDO index and documenting respective atmospheric and terrestrial anomalies over different parts of the globe (Gershunov and Barnett 1998; Pierce 2002; Roy et al. 2003; Goodrich 2007; Hu and Huang 2009).

Given the slow evolution of the OPDO, an analysis of the associated atmospheric response creates an impression that the relationship between the OPDO and atmospheric anomalies can also be used in a predictive mode; for example, knowing the phase of the OPDO this month might provide a skillful prediction of its atmospheric and terrestrial counterpart in subsequent months. This paradigm is analogous to the use of ENSO sea surface temperature (SST) indices and associated composites of surface temperature and precipitation obtained from the analysis of historical data in seasonal climate prediction efforts. To test whether a similar predictive relationship between the OPDO and its atmospheric counterpart exists, we examine the following question based on long coupled model simulations: Does knowing the OPDO index this month help predict atmospheric anomalies in subsequent months?

The scope of the paper is PDO variability on monthly time scales, rather than decadal ones as its name may imply. As will be demonstrated later, the autocorrelation of the monthly OPDO index is approximately 0.35 at a 4-month lead time; even though the OPDO has a higher persistence compared to the monthly mean atmospheric variability, the OPDO index can still have considerable month-to-month variability in line with the focus of the present analysis on monthly time scales.

Corresponding author address: Dr. Arun Kumar, 5830 University Research Court, NCWCP, College Park, MD 20740.
E-mail: arun.kumar@noaa.gov

DOI: 10.1175/JCLI-D-12-00057.1

The design of model simulations is outlined in section 2, and results are presented in section 3. Conclusions are summarized in section 4.

2. Model simulation

SST, 200-hPa geopotential heights (H200), surface temperature over land, and precipitation were analyzed from a set of 500-yr model simulations with the National Centers for Environmental Prediction (NCEP) Climate Forecast System (CFS) coupled model version 1 (Saha et al. 2006). The atmospheric model in the CFS has a horizontal resolution of T62 and 64 vertical levels. The ocean model has a horizontal resolution of 1° (longitude) by ⅓° (latitude) between 10°S and 10°N, and increases to 1° (latitude) poleward of 30°S and 30°N. There are 40 layers from 5 m below sea level to 4479 m, with a 10-m resolution in the upper 240 m. More details about the CFS can be found in Saha et al. (2006).

Analysis is based on two 500-yr coupled model simulations. As ENSO has an influence on the OPDO (Newman et al. 2003; Wang et al. 2012), to keep the analysis simple, the majority of results shown utilize data from a coupled simulation in which equatorial Pacific SST variability related to ENSO is suppressed. This is achieved by relaxing coupled model predicted SST to a SST climatology on a daily basis, and the relaxation is equivalent to nudging the model-produced SST to the daily SST climatology with an *e*-folding time of 3.3 days in the equatorial tropical Pacific (10°S–10°N, 140°E–75°W) [for more details, see Wang et al. (2012)]. The daily SST climatology was interpolated from long-term mean monthly SSTs derived from the National Oceanic and Atmospheric Administration (NOAA) Optimum Interpolation SST (OISST) version 2 (Reynolds et al. 2002) over the 1981–2008 period. The design of the simulation, therefore, is such that in an equatorial band in the tropical Pacific the SST is constrained to follow the seasonal cycle of observed climatology while elsewhere it is free to evolve based on coupled ocean–atmosphere interaction. Some results from this simulation were reported in Wang et al. (2012). Results based on the no-ENSO simulation are complemented by analysis of another 500-yr simulation where SST in all ocean basins (including the equatorial Pacific) is free to evolve and the ENSO variability in the tropical eastern Pacific is included (Zhang et al. 2007).

3. Results

a. Analysis of no-ENSO simulation

For the no-ENSO simulation, we first identify an atmospheric circulation pattern that is either responsible for or is associated with the OPDO-like SST pattern in the North Pacific. This is done in the following manner: empirical orthogonal function (EOF) analysis is used to find the dominant modes of model simulated monthly mean H200 variability over the North Pacific. Once these modes are obtained, the SST patterns that covary with different modes of height variability are found by regressing model simulated SSTs onto the principal component (PC) time series associated with the H200 EOFs. The regressed SST pattern that matches the known SST pattern associated with the ocean-based PDO index (i.e., the OPDO index) is then used to identify the atmospheric circulation pattern that is linked with the OPDO.

The SST pattern that is similar to the SST pattern associated with the oceanic signature of the PDO (Mantua et al. 1997) is shown in Fig. 1a. This pattern is obtained based on regression with the PC time series of one of the H200 EOFs (discussed below). The spatial structure of the SST has west-to-east oriented anomalies along 40°N, which are surrounded by U-shaped SST anomalies of opposite sign that start from the coast of Alaska and stretch along the west coast of North America down to 30°N, where they swing initially southward and then westward between 20° and 30°N. Indeed, based on the traditional approach of EOF analysis of the model simulated SST variability, a similar SST anomaly pattern associated with the OPDO variability in the North Pacific can also be obtained; this is shown in Fig. 1b. The spatial anomaly correlation between the two SST patterns, one based on the regression with the H200 variability and one based on the EOF of SST variability itself, is 0.90. We also note that there are some differences in the amplitude that may occur because the SST pattern in Fig. 1a is based on regression with the PC of H200 EOF while that in Fig. 1b is based on direct EOF analysis of the model simulated SST variability

In Fig. 1c the time series associated with the two SST patterns for a 100-yr segment is shown. The time series associated with the SST EOF (Fig. 1b) is merely the corresponding PC time series, while the time series associated with the H200-based SST pattern (Fig. 1a) is obtained by projecting the monthly mean SST onto the SST pattern in Fig. 1a. The two SST time series (which are inferred independently) have a very good correspondence with correlation over the 500-yr period of 0.95. Spectral analysis of the PC time series of the SST, and its comparison with the observed counterpart, was reported in Wang et al. (2012).

The mode of H200 variability (the PDO index based on the 200-hPa geopotential heights hereafter referred to as APDO) associated with the OPDO SST variability

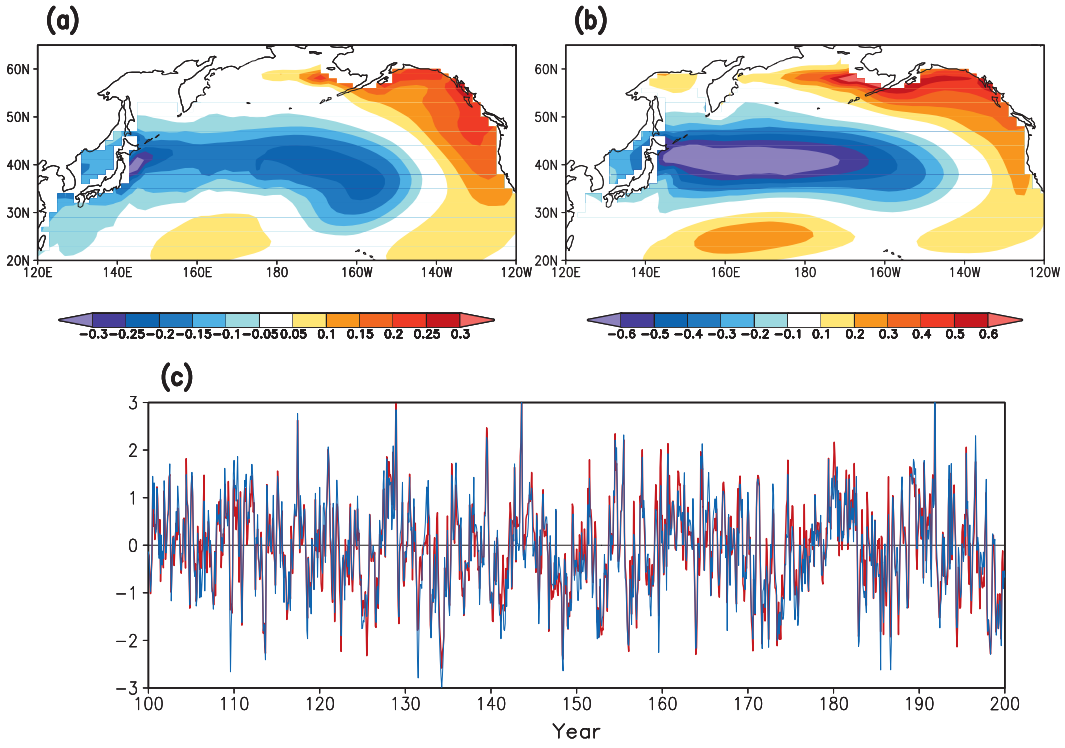

FIG. 1. SST anomalies (unit: K) associated with (a) EOF of H200 heights in Fig. 2b and (b) EOF of North Pacific SSTs, and (c) the normalized time series (red) based on projecting monthly mean SST anomalies onto the SST pattern in (a) and the PC time series (blue) associated with the SST EOF. For brevity, time series is only shown from years 100 to 200. EOFs of SST are computed over 20°–60°N, 125°E–100°W, and the EOF shown here is the second leading pattern of the EOF and explains 15% of monthly mean SST variability. The spatial patterns of SST anomalies in (a) and (b) are obtained by regressing monthly mean SST anomalies onto the PC time series of H200 (Fig. 2b) and the OPDO index based on the EOF of SST, respectively.

in Fig. 1a is shown in Fig. 2. Wang et al. (2012) demonstrated that surface wind variability associated with this pattern is the primary forcing for the SST pattern associated with the OPDO, a conclusion also supported by the analysis of Davis (1976), Frankignoul and Hasselmann (1977), Newman et al. (2003), Alexander (2010), Deser et al. (2010), and Pierce et al. (2001). The corresponding PC time series for a 100-yr segment shown in Fig. 2b indicates that this pattern has high month-to-month variability, and its lack of persistence is later quantified based on the autocorrelation analysis.

We next discuss the temporal characteristics of the OPDO and the APDO for the time series in Figs. 1c and 2b. The autocorrelation shown in Fig. 3a indicates that the APDO has little month-to-month persistence and the autocorrelation with one (two)-month lag drops to 0.2 (0.05). The time scale associated with OPDO variability is longer than for the APDO index (e.g., at a lag of four months the autocorrelation is 0.35).

The characteristic time scales associated with the APDO and OPDO are in concert with the existing notion of the OPDO variability; that is, the OPDO is a red noise response to the white noise stochastic atmospheric forcing (Pierce 2002). Following this notion, the OPDO time series has been successfully modeled based on two components: 1) persistence that is due to the thermal inertia associated with the ocean acting as an integrator of atmospheric forcing, and 2) atmospheric variability acting as a stochastic forcing (Liu 2011; Newman et al. 2003). In this paradigm, chance happenstances in the atmospheric variability [e.g., a preponderance of atmospheric variability (Fig. 2a) to randomly prefer a particular phase over a period of time] is what leads to the development of the corresponding phase of the OPDO in Fig. 1a (Hasselmann 1976). For the subsequent discussion, and to probe the question of whether knowing the OPDO index this month helps predict atmospheric anomalies in subsequent months, differences in the autocorrelation time scale for the APDO and the OPDO time series will play an important role.

We next analyze the lead–lag correlations for the APDO and the OPDO index time series (Fig. 3b). The structure of the lead–lag correlation is such that when the APDO index leads the OPDO index the correlation

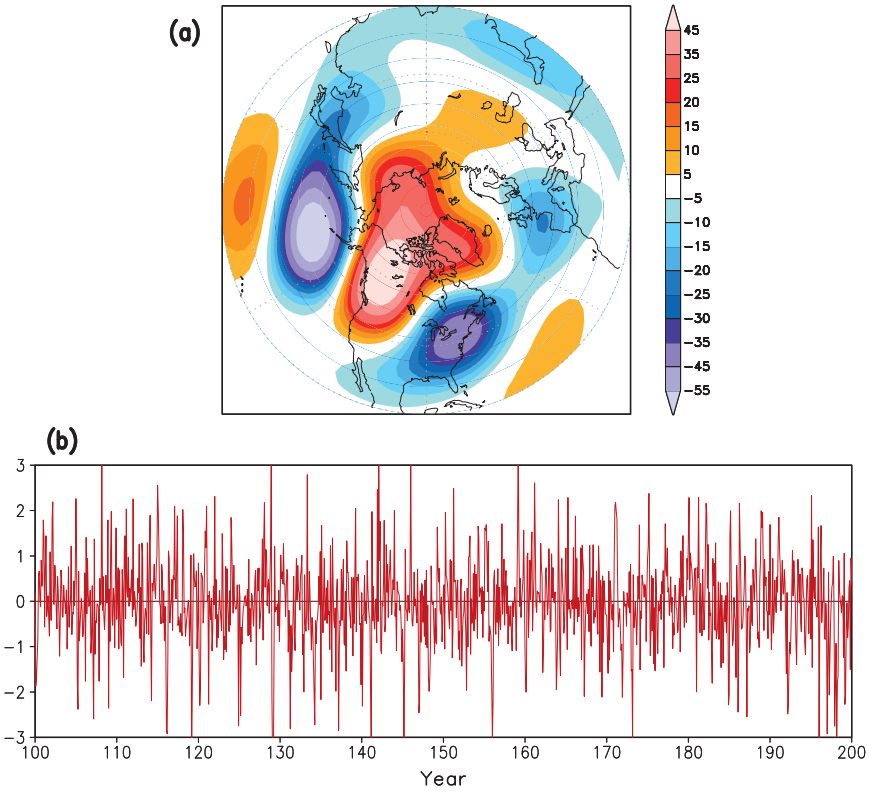

FIG. 2. (a) Spatial pattern of H200 height anomalies (unit: gpm) associated with leading EOF of H200 monthly mean height computed over the Pacific–North American region (20°–90°N, 150°E–30°W) and (b) corresponding normalized PC time series from years 100 to 200. The leading EOF explains 17% of monthly mean H200 height variability. The H200 height anomalies are obtained by regressing monthly mean height anomalies onto the PC time series.

is higher than the OPDO index leading the APDO index. This result motivates the conclusion that although the white noise atmospheric variability associated with the APDO is responsible for the OPDO, once the SST pattern associated with the OPDO is established it does not constrain the future state of the APDO variability.

The validity of the above conclusion is further illustrated from the lead–lag regression patterns for the North Pacific SST (Fig. 4) and H200 (Fig. 5) with the OPDO index. Consistent with the longer time scale for the OPDO, the associated SST pattern maintains the same spatial structure for various leads and lags, indicating a slow buildup in amplitude of SST to lag 0 and then a slow decay afterward.

For H200 (Fig. 5), however, it is only when H200 leads the OPDO index that the regression coefficients have significant amplitudes. Furthermore, the spatial structure of the H200 in Fig. 5 leading to the buildup of the OPDO is the same as in Fig. 2a.

Based on the analysis of the autocorrelation (Fig. 3a), the lead–lag correlation between the APDO and the OPDO time series (Fig. 3b), and the lead–lag regression of SST and H200 anomalies with the OPDO index (Figs. 4 and 5), the following conclusions are made: 1) the SST structure corresponding to the OPDO index varies on a slow time scale and, given the OPDO index this month, one can anticipate its value (and the corresponding SST structure) during the subsequent months based on persistence as a forecast; and 2) the simultaneous atmospheric regression pattern (Fig. 2a) associated with the OPDO may not have any predictive value for atmospheric anomalies in subsequent months. This is because the atmospheric variability remains a stochastic noise and is not constrained by the SST forcing associated with the OPDO; even though the SST pattern is established by the atmospheric variability associated with the APDO, the same SST forcing does not constrain the APDO variability in subsequent months. This result is consistent with studies that found a weak influence of extratropical SSTs on atmospheric variability (Delworth 1996; Lau and Nath 1996; Barsugli and Battisti 1998; Robinson 2000; Kumar et al. 2008; Jha and Kumar 2009) and analysis by Pierce (2002) in the context of PDO variability.

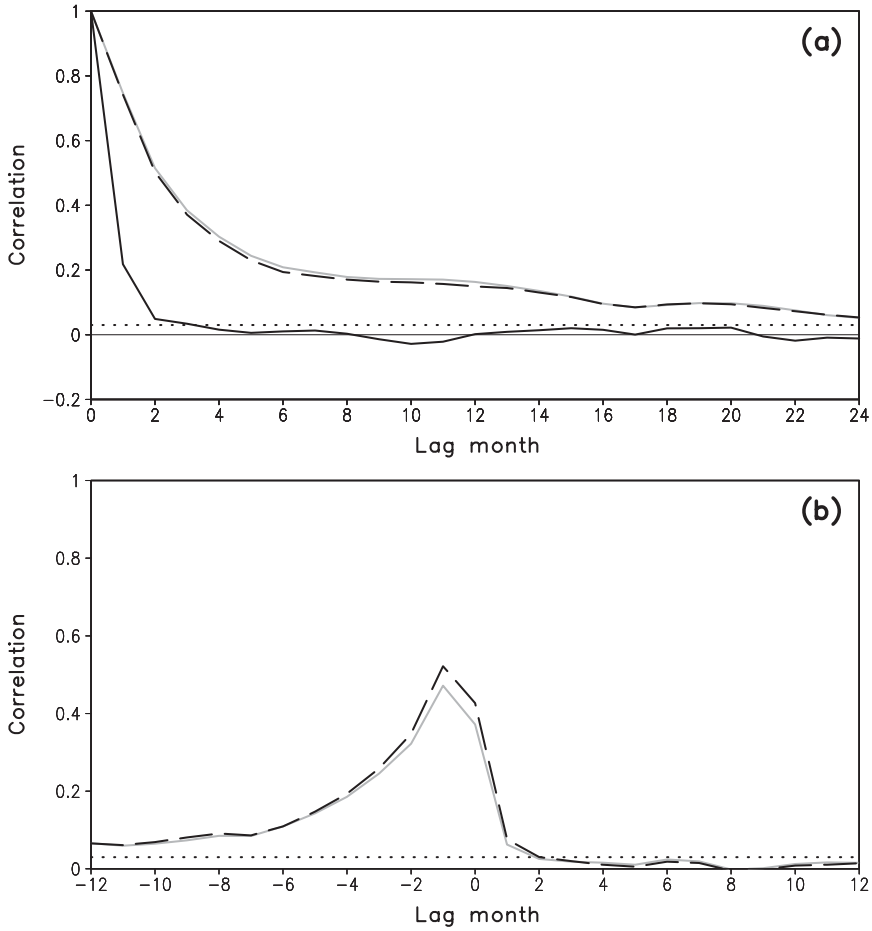

FIG. 3. (a) Autocorrelations for the 500-yr-long monthly PC time series of H200 height EOF (black solid line), the OPDO index based on the SST EOF (gray solid line), and the time series of SST projection coefficient (black dashed line). (b) Lead–lag correlations between the 500-yr monthly PC time series of H200 height EOF and the OPDO index (gray solid) and that with the time series of SST projection coefficients (black dashed line). Negative lags in (b) mean that the H200 heights are leading the SST. Dotted lines in (a) and (b) indicate the 99% significance level, estimated by the Monte Carlo test.

The lack of predictive utility of atmospheric anomalies associated with the OPDO is in contrast to the predictive nature of atmospheric composites associated with ENSO variability. It is well established through analysis of both the historical observational data and atmospheric general circulation model simulations that SST variability associated with ENSO forces global atmospheric anomalies. Because of the slow evolution of ENSO-related SST anomalies, these atmospheric teleconnection patterns can be used in a predictive sense. In other words, a combination of knowing the ENSO SST patterns (and associated index) this month, and the knowledge of atmospheric teleconnection patterns associated with ENSO, does provide predictive capability. Indeed, such an approach was a catalyst for initiating seasonal climate prediction efforts (Horel and Wallace 1981; Kumar et al. 1996; Trenberth et al. 1998).

To illustrate that OPDO-related atmospheric anomalies indeed have little to no potential predictability, we create a prediction of H200 anomalies based on a linear reconstruction with the OPDO index. The linear reconstruction is based on the simultaneous regression of the H200 pattern onto the OPDO index, which is basically the H200 pattern in Fig. 2a. The anomaly correlation map between the linearly reconstructed and model simulated monthly mean H200 is shown in Fig. 6a. The spatial pattern of anomaly correlation matches the regression pattern in Fig. 5. Although there is a good match in the spatial pattern, the reason that maximum anomaly correlation is not always proportional to the

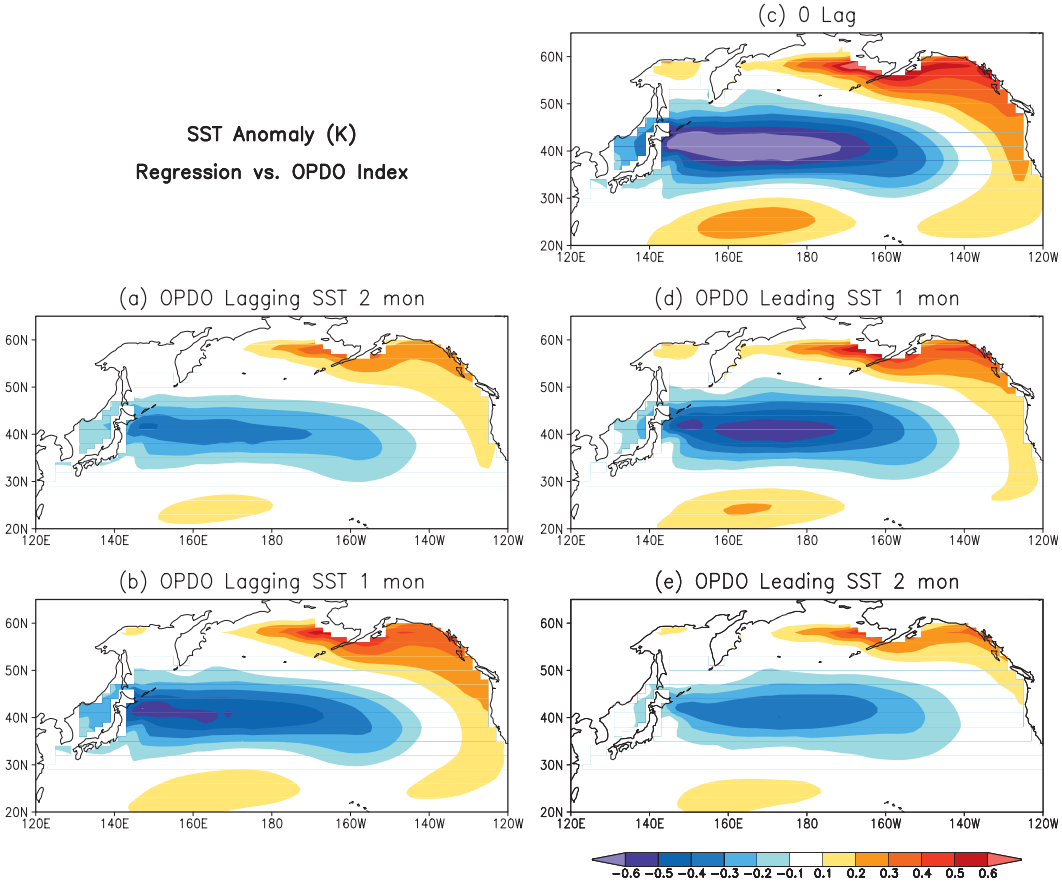

FIG. 4. Regression patterns of SST anomalies (K) associated with one standard deviation departures of the PC time series of the OPDO index for OPDO lagging SST by (a) 2, (b) 1, and (c) 0 months, and for the OPDO leading SST by (d) 1 and (e) 2 months.

amplitude of height anomaly itself is because the anomaly correlation depends on the amplitude of regressed signal relative to the noise (Kumar and Hoerling 2000). Prediction skill (or alternatively, the potential predictability as the analysis is done within the context of model simulations) of H200 anomalies with one-month lead is negligible [i.e., using this month's reconstructed pattern as the prediction for next month's model, the simulated H200 has a much smaller anomaly correlation (Fig. 6b)]. Use of reconstructed H200 based on a pattern where the OPDO index leads the H200 does not help as the amplitude of this pattern itself is much smaller (Figs. 5d,e). We also note that although the skill with one month lead is much smaller, there is a region with small skill near the western portion of SST in Figs. 1a and 1b. This region associated with the western boundary currents has been noted as one of the strongest candidates for possible atmospheric response to SST variability (Kwon et al. 2010; Frankignoul et al. 2011).

The analysis of the no-ENSO simulation so far was based on the assumption of linearity (i.e., linear regression) and also did not differentiate seasonality in OPDO and APDO. We next demonstrate that the main conclusion of the analysis (i.e., knowing the OPDO index does not have predictive value for atmospheric anomalies in subsequent months) still holds when these factors are taken into account.

Figure 7 shows the lead–lag H200 response based on composites (an approach that does not involve any assumption about the linearity). For this analysis, the months when the absolute value of the OPDO index exceeds one standard deviation were first identified. Lead and lag H200 composites were then created with respect to these months for positive and negative phases of the OPDO. The general feature of lead–lag H200 composites for both phases of the OPDO is the same as the regression-based analysis in Fig. 5 and the H200 has larger amplitude when the OPDO index lags the H200, but has little amplitude when the OPDO index leads the H200. An interesting point to note is that for the opposite phases of the OPDO, the H200 composites themselves have a fair amount of symmetry.

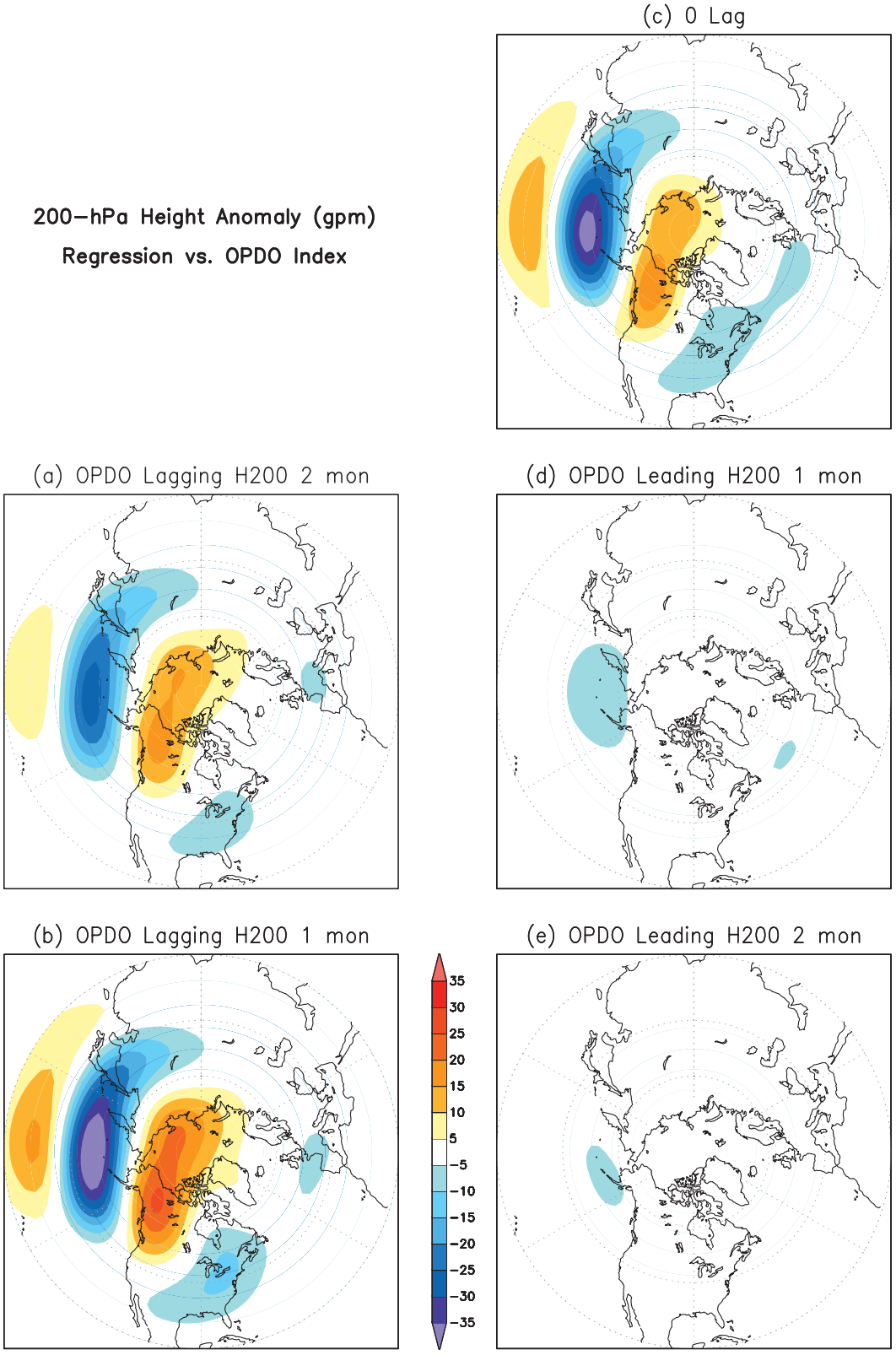

FIG. 5. Regression patterns of H200 height anomalies (gpm) associated with one standard deviation departures of the PC time series of the OPDO index for the OPDO lagging H200 height by (a) 2, (b) 1, and (c) 0 months, and for the OPDO leading H200 by (d) 1 and (e) 2 months.

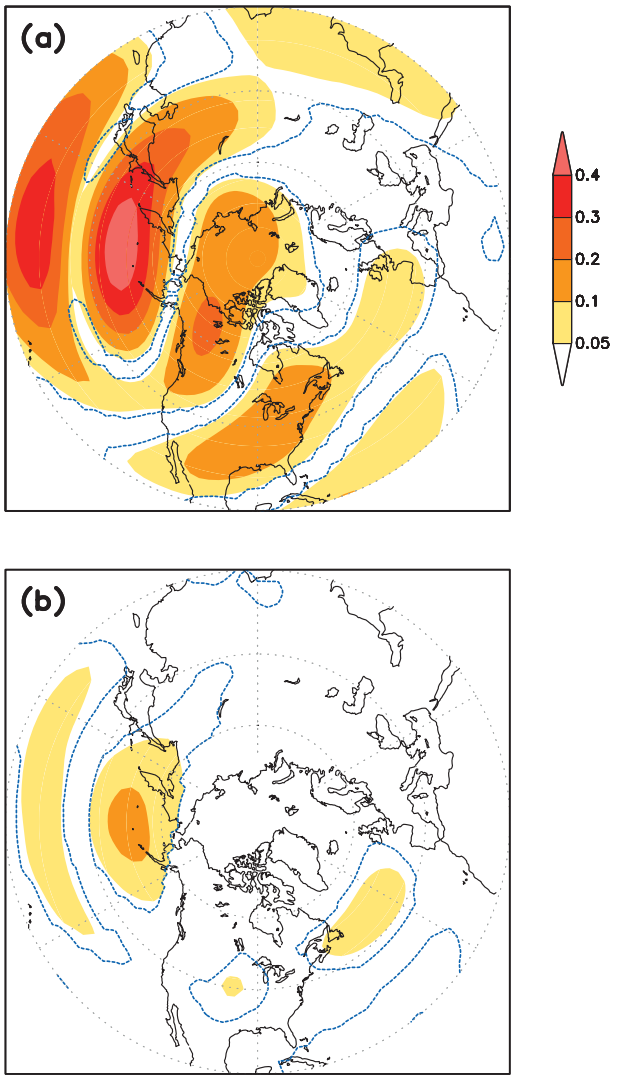

FIG. 6. Anomaly correlation between model-simulated and reconstructed H200 height fields (a) over the entire 500 yr and (b) when reconstructed H200 height leads model simulated H200 height by one month. The reconstructed H200 height anomalies are obtained based on the OPDO index and its regression against the model H200 height anomalies. Blue contours indicate the 99% significance level, estimated by the Monte Carlo test.

The analysis in Fig. 5 (that was over the annual cycle) is next repeated just for the months of December–February (DJF) and June–August (JJA) (Fig. 8). The analysis procedure is the same as for Fig. 5 except the lead–lag H200 anomalies are regressed over these months only (instead of regressed over all months of the year). Regarding the predictive value of the OPDO index, once again similar results hold for the analysis over DJF and JJA in that when the OPDO index leads H200, the amplitude of H200 anomalies is much smaller. Between boreal winter and summer seasons there are differences in the spatial structure of H200 with the winter pattern being better defined and having a spatial structure with longer wavelength, a feature that is typical for wintertime circulation anomalies (Barnston and Livezey 1987).

Conclusions similar to H200 also hold for surface quantities, and examples of variables of societal relevance—surface temperature and precipitation—are shown in Fig. 9, where lead–lag regressions similar to H200 in Fig. 5 are shown. Consistent with H200, the fingerprint of the OPDO index on these variables is larger when the OPDO index lags versus when the OPDO index leads. This is consistent with the notion that the variability in H200 is the link that is common between oceanic and terrestrial anomalies, and the reason atmospheric circulation is often referred to as the "atmospheric bridge" that provides an apparent connection between anomalies over different regions (Alexander et al. 2002). Following this notion, while H200 anomalies (Fig. 2a) are responsible for forcing the OPDO SST, at the same time they are also responsible for the surface temperature and precipitation anomalies over the land. However, once the OPDO SST is established and no longer constrains the H200 variability in the future, the associated anomalies of surface temperature and precipitation also diminish.

b. *Analysis of the ENSO simulation*

The extratropical atmospheric response to the tropical ENSO SST anomalies also projects onto the pattern of atmospheric variability that is responsible for the OPDO (i.e., H200 in Fig. 2a) and ENSO variability has been documented to influence the OPDO variability (Newman et al. 2003; Wang et al. 2012). The commingling of the influence of ENSO and the atmospheric internal variability on the OPDO complicates the analysis of the OPDO variability, and for that reason the analysis in the previous section was based on the no-ENSO simulation. To illustrate that the presence of ENSO variability in the equatorial tropical Pacific does not alter the fundamental relationship between the OPDO and the APDO, some selected analysis from a 500-yr simulation with ENSO is presented next.

For the ENSO simulation two sets of analysis are done. In the first set the OPDO and the APDO indices are derived based on the raw model output of monthly means (similar to that in the previous section) and therefore their variability contains the combined influence of atmospheric internal variability (as was the case for the no-ENSO simulation) and a component that is forced by ENSO. In the second set of analyses, we first linearly remove the ENSO-related component from the monthly means of ocean and atmospheric anomalies and then compute the OPDO and APDO

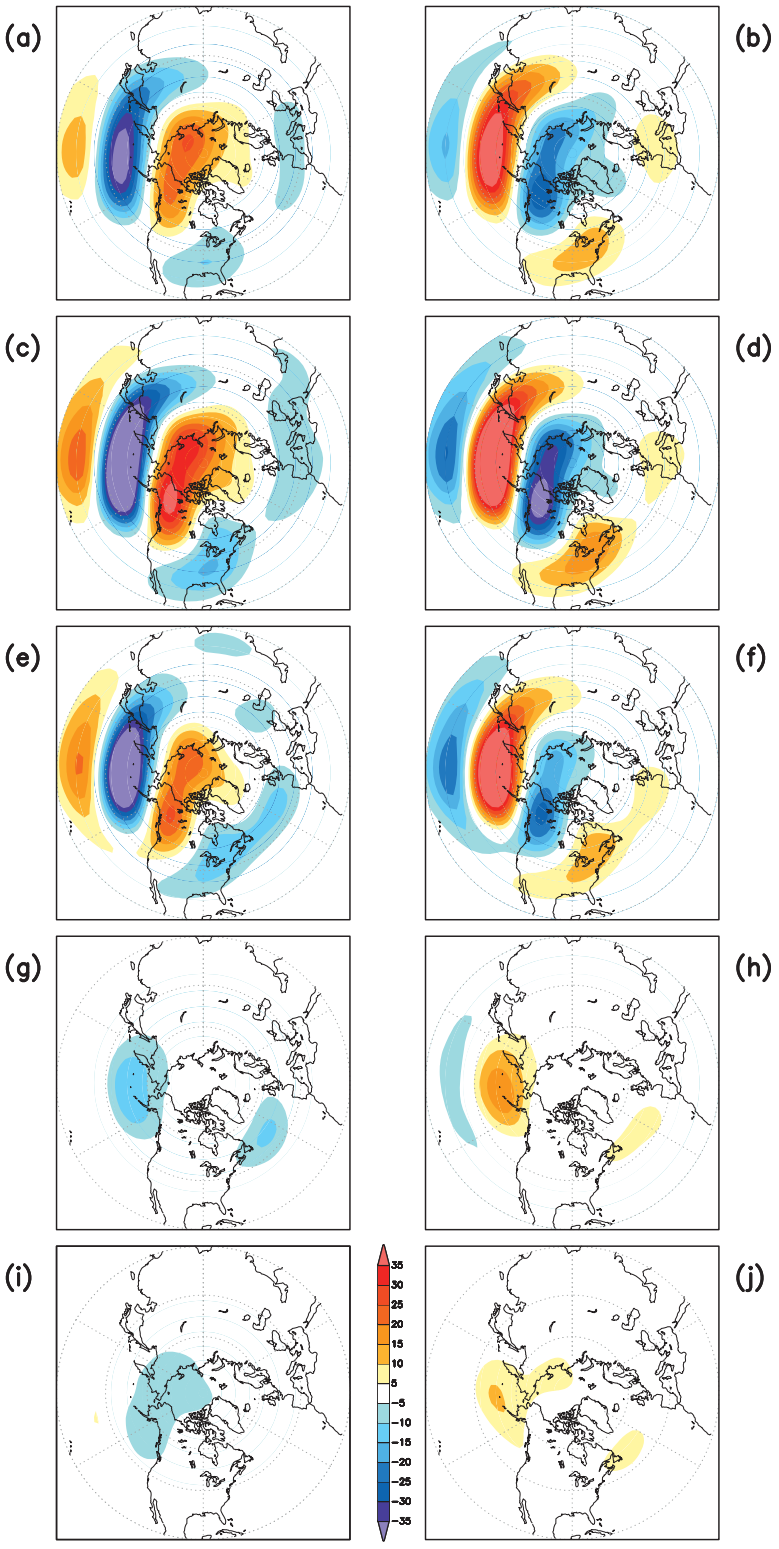

FIG. 7. As in Fig. 5, but following the composite analysis approach. The left (right) columns are H200 composites (gpm) for the monthly OPDO index greater (less) than positive (negative) one standard deviation positive, when the then OPDO lags H200 by (a),(b) 2, (c),(d) 1, and (e),(f) 0 months, and when the OPDO leads H200 by (g),(h) 1 and (i),(j) 2 months.

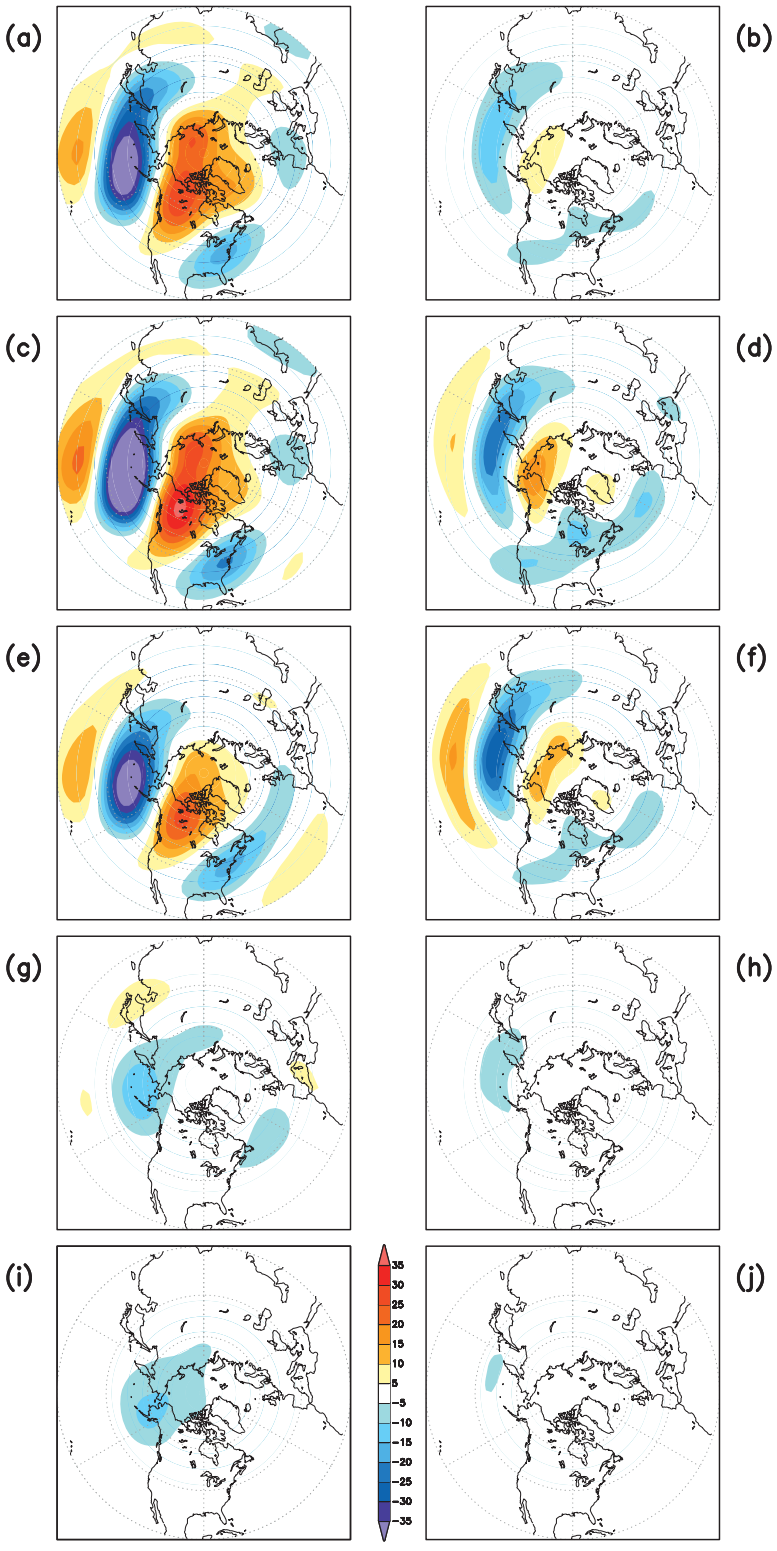

FIG. 8. Regression patterns of H200 anomalies (gpm) associated with one standard deviation departures of the PC time series of the OPDO index for (left) DJF and (right) JJA, when the OPDO lags H200 by (a),(b) 2, (c),(d) 1, and (e),(f) 0 months, and when the OPDO leads H200 by (g),(h) 1 and (i),(j) 2 months.

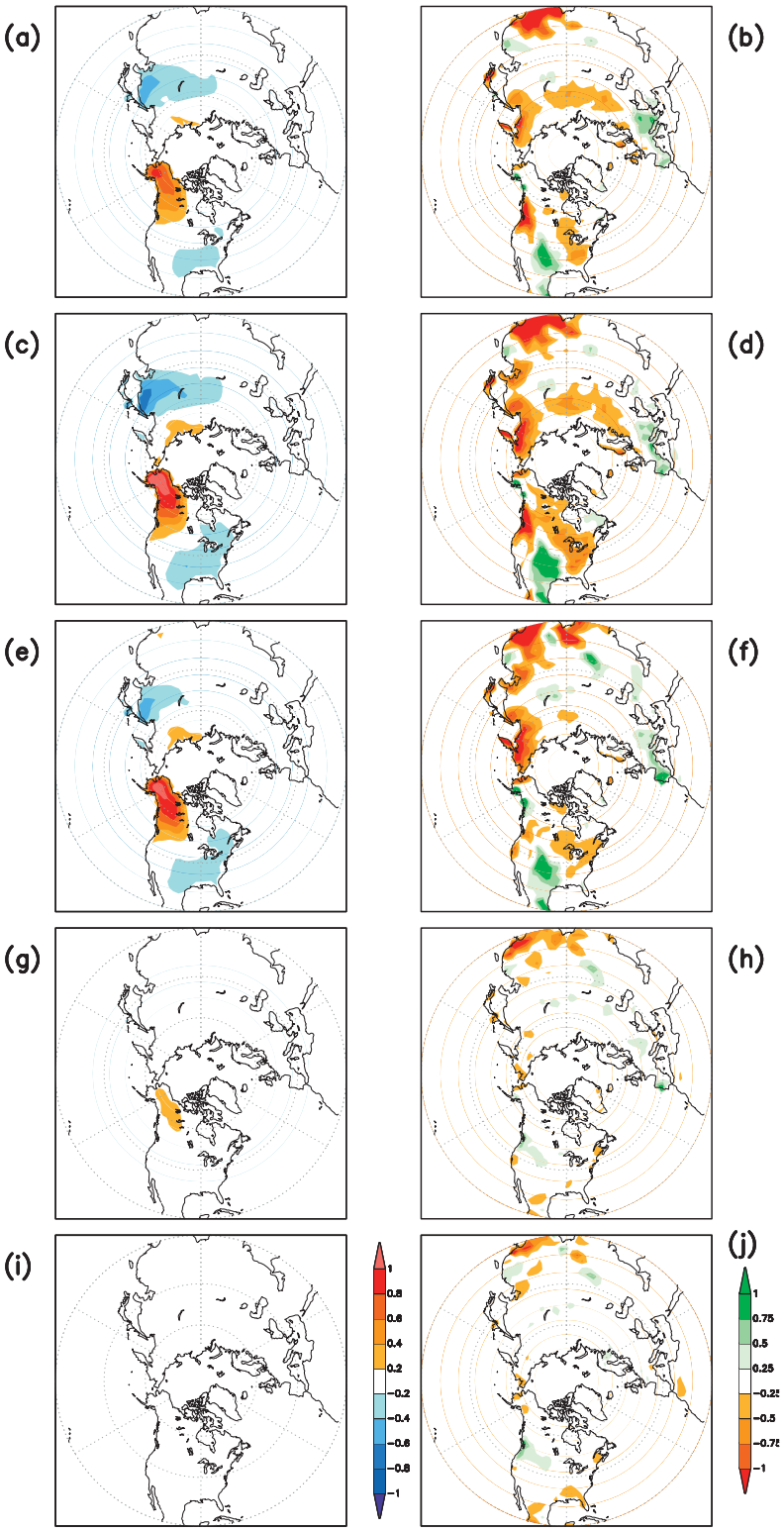

FIG. 9. As in Fig. 5, but for regression patterns of (left) surface temperature anomalies (°C) and (right) precipitation (0.1 mm day^{-1}) associated with one standard deviation departures of the PC time series of the OPDO index when the OPDO lags H200 by (a),(b) 2, (c),(d) 1, and (e),(f) 0 months, and when the OPDO leads H200 by (g),(h) 1 and (i),(j) 2 months.

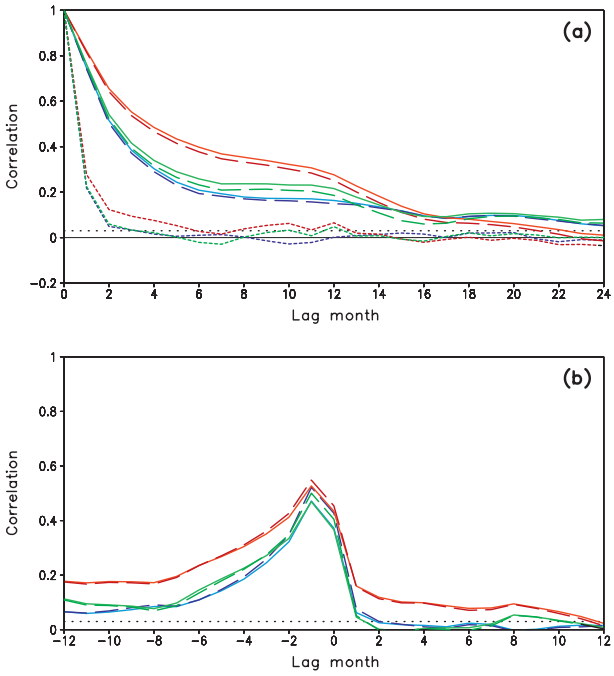

FIG. 10. As in Fig. 3; the additional lines are autocorrelation and lead–lag correlation for the ENSO simulation (red), and ENSO simulation but after linearly removing the ENSO component (green; see text for more details). Corresponding analysis for the no-ENSO simulation is also shown (blue) and is the same as in Fig. 3. Dotted lines are for the APDO index and solid lines for the OPDO index. Black dotted lines indicate the 99% significance level, estimated by the Monte Carlo test.

indices based on the EOF of residual monthly means. The removal of the ENSO-related signal follows a simple procedure where a reconstruction based on the regression between Niño-3.4 SST index and monthly mean of ocean and atmospheric anomalies is removed from the original monthly mean data.

In Fig. 10 the autocorrelations (top panel) and lead–lag correlations (bottom panel) between the OPDO and the APDO indices for both sets of calculations are shown. When the influence of ENSO is included, the autocorrelation for both APDO and OPDO indices has a somewhat slower decay than for the no-ENSO simulation. This is to be expected since ENSO SST anomalies in the equatorial tropical Pacific (which have a long time scale) impart a persistent forcing on the APDO, thereby tilting its probability to be more in a particular phase and resulting in a longer persistence time scale. A longer persistence in the APDO then also leads to a longer time scale for the OPDO index compared to that for the no-ENSO simulation.

For the analysis when the ENSO signal is linearly removed, the autocorrelations for both the APDO and the OPDO indices, however, are much closer to the ones for the no-ENSO simulation (Fig. 3, top), indicating that a linear superposition of the contribution due to the ENSO response and due to the atmospheric internal variability on the temporal characteristics of these indices may be a good approximation (Wang et al. 2012).

With the ENSO variability, similar to the analysis for the autocorrelation, the lead–lag correlation (Fig. 10b) is somewhat higher between the two indices and furthermore has a slightly higher correlation when the OPDO index leads the APDO index. This is a consequence of the OPDO index having a higher chance to be in phase with the subsequent values of the APDO index that could now be sustained by the slowly varying ENSO SST forcing. However, once the ENSO influence from both the indices is removed, the lead–lag correlation is smaller and has values similar to that for the no-ENSO simulation.

For the ENSO simulation we repeat the analysis in Fig. 5 to assess the lead–lag response in H200, and to see if conclusions similar to that for the no-ENSO simulation hold. The result from this analysis is shown in Fig. 11 (left column). Similar to that for the no-ENSO simulation, there is substantial decrease in amplitude in H200 when the OPDO index leads height anomalies. However, consistent with the higher correlation shown in Fig. 10, the amplitude of H200 is larger than the corresponding amplitude for the no-ENSO simulation (Fig. 5). This discrepancy is accounted for after the ENSO signal is linearly removed (Fig. 11, right column), indicating that the larger amplitude for H200 (lagging the OPDO index) occurs because of the influence of ENSO, and not because of the OPDO index having larger influence on the atmospheric circulation in the presence of ENSO. This analysis indicates that the fundamental relationship between the OPDO and APDO is retained in the presence of ENSO.

Can the information about the OPDO-related SST help improve seasonal prediction based on ENSO alone? In the traditional approach for ENSO-based seasonal prediction, atmospheric composites for different phases of ENSO (e.g., El Niño or La Niña) are used as specifications for the future state of the atmosphere once the future state of ENSO itself is anticipated. Will adding the information about the current state of the OPDO improve the prediction based solely on ENSO? In other words, can ENSO composites conditional to the state of the OPDO be more useful for seasonal prediction? Based on the analysis of 500-yr ENSO simulation, we demonstrate that this is not the case.

We consider the positive phase of the ENSO – El Niño and construct composites conditional to the phase of the OPDO index. This approach splits all El Niños (defined as when the Niño-3.4 SST index exceeds unit standard

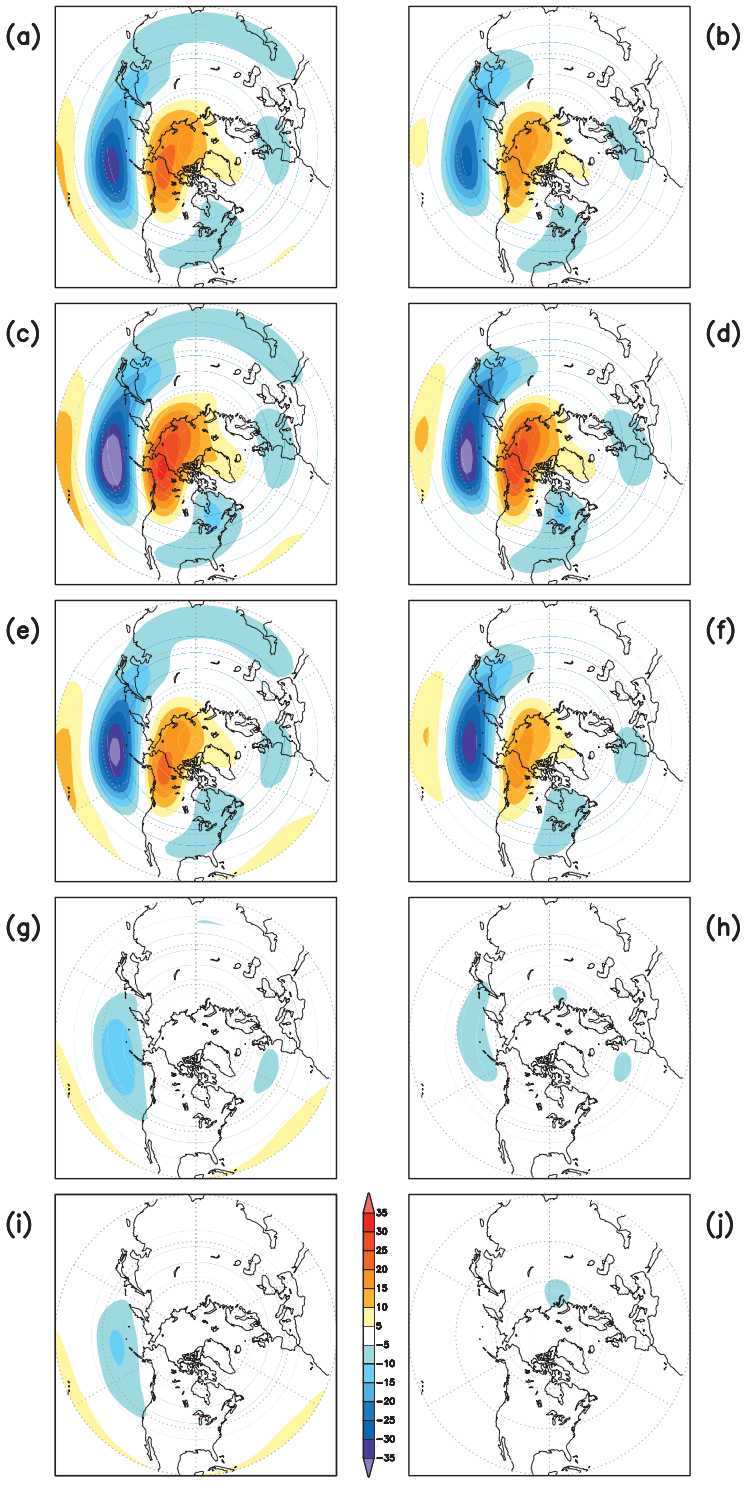

FIG. 11. As in Fig. 8, but for patterns of H200 anomalies (gpm) associated with one standard deviation departures of the PC time series of the OPDO index in the ENSO simulation. As for Fig. 5, the analysis is over the annual cycle. Values on the left are for the monthly mean from the ENSO simulation; values on the right are based on the analysis after linearly removing the ENSO signal from monthly mean H200 and SST; data are for when OPDO lags H200 by (a),(b) 2, (c),(d) 1, and (e),(f) 0 months, and when the OPDO leads H200 by (g),(h) 1 and (i),(j) 2 months.

deviation) in the 500-yr simulation into ones when the OPDO index is positive and when OPDO index is negative, and constructs two separate atmospheric composites for the El Niño conditional to the state of the OPDO.

Lead–lag H200 El Niño composites for the two phases of the OPDO index are shown in Fig. 12. The left (right) column is for the positive (negative) OPDO index when H200 anomalies associated with the respective phase of the OPDO are in (out of) phase with the extratropical response to El Niño. The main difference between the two El Niño H200 conditional composites is when the OPDO index lags the H200—that is, when atmospheric circulation anomalies associated with the APDO are responsible for the establishment of the SST anomalies associated with the corresponding OPDO index. Beyond lag zero, however, when either phase of the OPDO index does not constrain the APDO index, the conditional H200 El Niño composites are similar, and furthermore are basically the unconditional El Niño H200 composite (not shown). The difference between the two El Niño composites in Fig. 12 is also consistent with the linear superposition of the unconditional El Niño H200 composite and H200 composites associated with the two phases of the OPDO index (analysis not shown).

After the demonstration that concurrent knowledge of the El Niño and OPDO index does not help improve seasonal prediction of atmospheric anomalies, the last issue we discuss is the El Niño composites conditioned to the low-frequency (LF) phase of the OPDO. This discussion is in light of results discussed by Gershunov and Barnett (1998), who reported differences in ENSO teleconnection in extratropical latitudes during different LF phases of the OPDO index. The LF OPDO time series used in this study is obtained by processing the 500-yr monthly OPDO index through a Lanczos low-pass filter (Duchon 1979) with a cutoff period of 8 years. The filtered OPDO time series highlights the LF evolution of the OPDO and excludes month-to-month and interannual variations.

Although the autocorrelation of the monthly OPDO index is small (Fig. 3), the OPDO can preferentially stay in one phase for an extended period of time (see the OPDO time series in Fig. 1). This can be confirmed based on the spectral analysis of the monthly OPDO index having a significant energy in long time scales [see Wang et al. (2012) for the spectral analysis of the OPDO index for the simulations used in this paper]. If the stochastic atmospheric variability (i.e., the APDO) is the primary forcing for the OPDO, then the LF component of the OPDO is merely a consequence of the APDO being in a particular phase more often by chance alone.

With this basic premise, the influence of LF variability of the OPDO on the ENSO composite is discussed. For a long enough time series (as is the case for the model simulations) one can construct El Niño composites conditional to the LF phases of the OPDO (Gershunov and Barnett 1998). By construction, El Niño composites (which are based on monthly variability of the Niño-3.4 SST index) in the positive (negative) LF phase of the OPDO will also have a preponderance of the positive (negative) phase of the corresponding OPDO index, and consequently will have a larger probability for the APDO (which forces the OPDO) to be in the phase consistent with the LF phase of the OPDO index. We confirmed that atmospheric composites for El Niño conditional to the positive and negative LF phases of the OPDO index do indeed differ (not shown), and the difference is mainly in the amplitude of the unconditional El Niño composite that is modulated by the mean circulation anomalies corresponding to the LF phase of the OPDO. This should not come as a surprise since any subcategorization of El Niño based on an independent index will contain the atmospheric signature corresponding to that index. For example, to construct El Niño composites conditional to the LF phase of the North Atlantic Oscillation (NAO), the resulting atmospheric composites will contain the atmospheric fingerprint of the NAO.

We have already discussed that added information of the monthly OPDO index does not add to the prediction based on the El Niño index. The question we now pose is whether the differences in the El Niño composites for different LF phases of the OPDO index have a predictive capability. To assess the potential predictability (or the skill) of H200 anomalies due to El Niño-based conditional and unconditional H200 composites, an anomaly correlation analysis similar to Fig. 6 was done. The anomaly correlation computed over El Niño events and based on various ENSO composites (i.e., conditional and unconditional) is shown in Fig. 13. The analysis procedure is as follows: 1) monthly mean H200 anomalies for December is predicted based on knowing the Niño-3.4 SST index and the LF phase of the ODPO in the months of November or October (i.e., using lagged value for the indices), 2) the corresponding H200 unconditional or conditional composite are specified as the prediction, and 3) a similar procedure for H200 prediction is repeated for the months of January and February, and then anomaly correlation between the model simulated and predicted H200 is computed over the El Niño years. The general procedure for obtaining H200 El Niño composites conditional to the LF phase of the OPDO is the same as for the monthly OPDO index except that the separation of El Niños into two categories is now according to the sign of the LF phase of the OPDO.

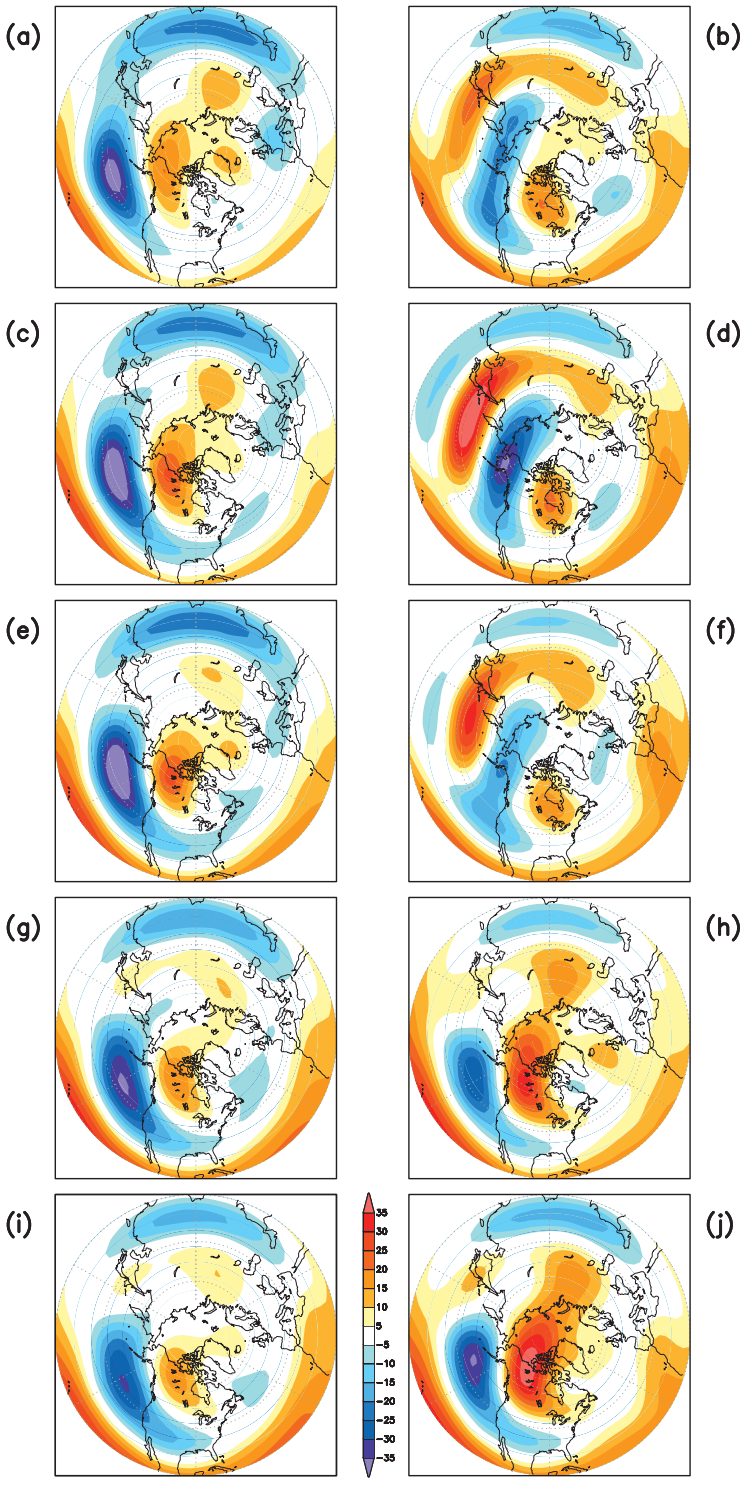

FIG. 12. As in Fig. 11, but for H200 (gpm) composites based on the Niño-3.4 SST index greater than one standard deviation (i.e., El Niño events) in the model simulation. On the left (right) are shown H200 composites when in addition to a Niño-3.4 SST index greater than one standard deviation, the monthly OPDO index is also greater (smaller) than positive (negative) one standard deviation. Data are for when the OPDO lags H200 by (a),(b) 2, (c),(d) 1, and (e),(f) 0 months, and when the OPDO leads H200 by (g),(h) 1 and (i),(j) 2 months.

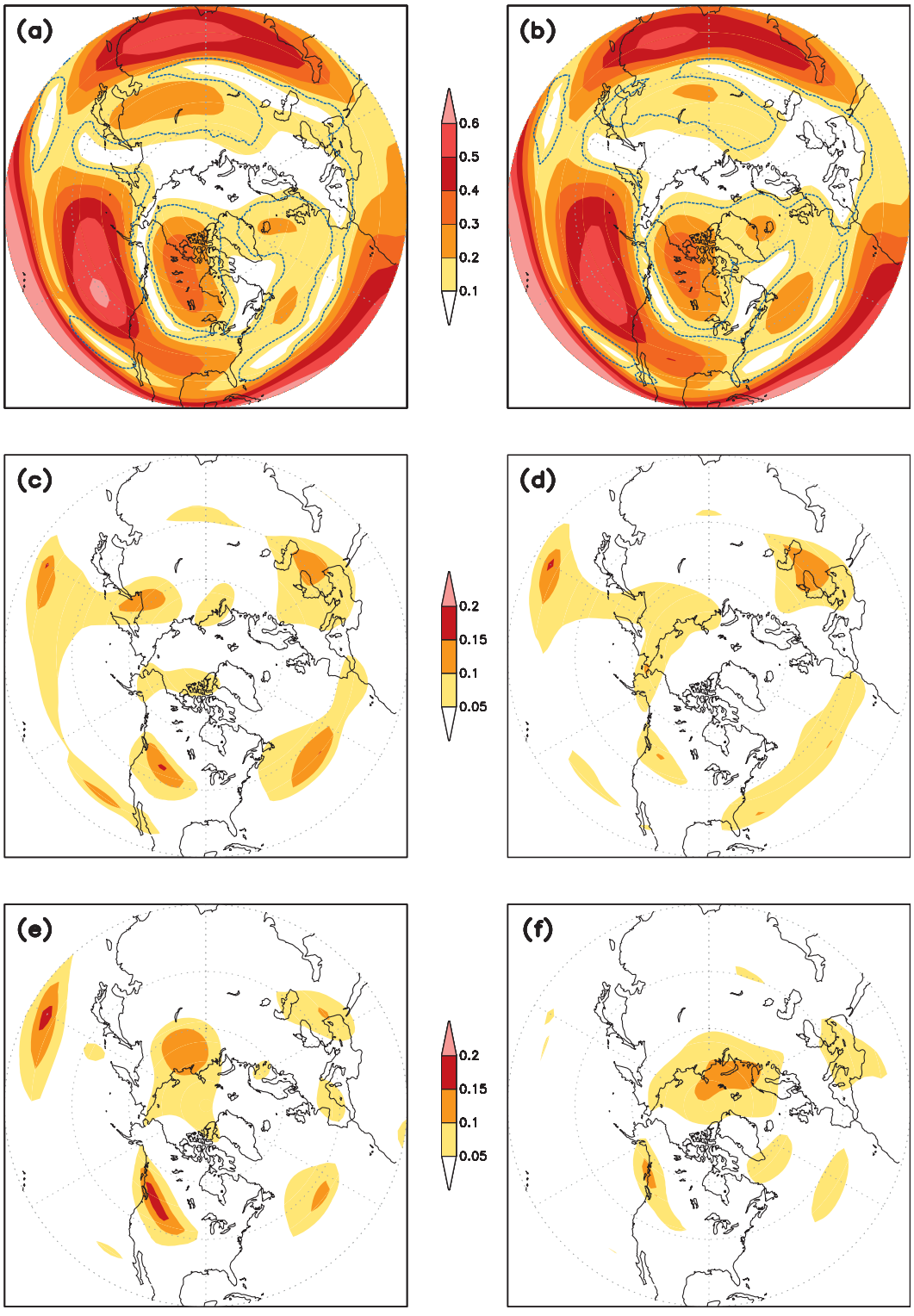

FIG. 13. Spatial map of anomaly correlation between model-simulated H200 and specification of various H200 composites as the prediction, showing prediction of DJF anomalies with (left) zero- and (right) one-month lead. Shown are (a),(b) anomaly correlation for unconditional El Niño composite as the forecast; (c),(d) the difference between anomaly correlation for El Niño composite that is conditioned to the low-frequency phase of the OPDO as the forecast and that in (a) and (b), respectively; and (e),(f) the difference between anomaly correlation for El Niño composite that is conditioned to the difference phase of the monthly OPDO index and that in (a) and (b), respectively. Blue contour indicates the 99% significance level, estimated by the Monte Carlo test.

The anomaly correlation for the unconditional El Niño composite for zero month lead prediction (where H200 for December–February was based on H200 composites corresponding to the Niño-3.4 SST index for November–January) and for one-month lead prediction (where H200 for December–February was predicted based on H200 composites corresponding to Niño-3.4 SST index for October–December) (Fig. 13, top panels) show a spatial pattern consistent with the El Niño composite with largest skill in the tropical latitude and over the Pacific–North American (PNA) region. The difference in skill for the H200 El Niño composites conditioned on the LF phase of the OPDO (Fig. 13, middle panels) indicates that the skill is slightly higher, but not significantly different from that for the unconditional composites. For the sake of completeness the difference in anomaly correlation for the H200 El Niño composites, now conditioned to the phase of the monthly (unfiltered) OPDO index (as in Fig. 12), is shown in the bottom panels (Fig. 13). Consistent with the discussion related to Fig. 12, knowledge of the phase of the monthly OPDO index adds little to the prediction skill.

We note that skill assessment for the ENSO conditional to the LF phase of the OPDO index has a conceptual problem about its interpretation. This issue was highlighted by Bretherton and Battisti (2000). The time series of the OPDO is forced by the stochastic variability associated with the APDO and is a consequence of a unique realization of the APDO over a time history. However, to actually predict the LF phase of the OPDO over a long period of time, and use it to augment predictions based on the ENSO alone, would require predicting the monthly sequence of the history of the APDO. Given the dominant stochastic nature of the APDO variability, that task may not be feasible.

4. Conclusions

In this analysis we demonstrated that knowing the PDO index based on the SST variability (i.e., the OPDO index) does not lead to predictive value for atmospheric anomalies. Although the understanding of OPDO variability as a red noise ocean response to white noise atmospheric forcing has been discussed in literature, its implication for predicting the future state of the atmosphere itself has been confusing. Part of this confusion stems from the fact that since the OPDO index varies on a slow time scale similar to ENSO, it is assumed that, like ENSO, the simultaneous atmospheric teleconnection pattern associated with the OPDO will be of predictive value in subsequent months. However, as the results indicate, since the OPDO index does not constrain the atmospheric variability (which remains a white noise), the OPDO index on its own does not have predictive usefulness for atmospheric variability. Finally, this conclusion also holds for the simulation in which ENSO variability was included. The analysis reported in this paper was based on a single model, and although is supported by previous results (e.g., Pierce 2002; Newman et al. 2003) it needs to be further substantiated based on other model simulations. Additionally, the CFS has some deficiencies in simulating the variability of the OPDO. As documented in Wang et al. (2012), the peak of the power spectra for the OPDO in the ENSO run is weaker than the observations at both the interannual and decadal time scales. However, the model deficiencies should not alter the cause and effect relationship between the OPDO and APDO discussed in this paper, but they need to be verified based on other model simulations.

Acknowledgments. We thank Michael Halpert, Dr. Amy Bulter, Dr. Dimitry Smirnov, two anonymous reviewers, and the editor for constructive comments and suggestions.

REFERENCES

Alexander, M. A., 2010: Extratropical air–sea interaction, SST variability, and the Pacific decadal oscillation (PDO). *Climate Dynamics: Why Does Climate Vary?, Geophys. Monogr.*, Vol. 189, Amer. Geophys. Union, 123–148.

——, I. Bladé, M. Newman, J. R. Lanzante, N.-C. Lau, and J. D. Scott, 2002: The atmospheric bridge: The influence of ENSO teleconnections on air–sea interaction over the global oceans. *J. Climate,* **15,** 2205–2231.

Barnston, A. G., and R. E. Livezey, 1987: Classification, seasonality and persistence of low-frequency atmospheric circulation patterns. *Mon. Wea. Rev.,* **115,** 1083–1126.

Barsugli, J. J., and D. S. Battisti, 1998: The basic effects of atmosphere–ocean thermal coupling on midlatitude variability. *J. Atmos. Sci.,* **55,** 477–493.

Bretherton, C. S., and D. S. Battisti, 2000: An interpretation of the results from atmospheric general circulation models forced by the time history of the observed sea surface temperature distribution. *Geophys. Res. Lett.,* **27,** 767–770.

Davis, R. E., 1976: Predictability of sea surface temperature and sea level pressure anomalies over the North Pacific Ocean. *J. Phys. Oceanogr.,* **6,** 249–266.

Delworth, T. L., 1996: North Atlantic interannual variability in a coupled ocean–atmosphere model. *J. Climate,* **9,** 2356–2375.

Deser, C., M. A. Alexander, S.-P. Xie, and A. S. Phillips, 2010: Sea surface temperature variability: Patterns and mechanisms. *Annu. Rev. Mar. Sci.,* **2,** 115–143.

Duchon, C. E., 1979: Lanczos filtering in one and two dimensions. *J. Appl. Meteor.,* **18,** 1016–1022.

Frankignoul, C., and K. Hasselmann, 1977: Stochastic climate models, Part II: Application to sea-surface temperature variability and thermocline variability. *Tellus,* **29,** 289–305.

——, N. Sennechael, Y.-O. Kwon, and M. A. Alexander, 2011: Influence of the meridional shifts of the Kuroshio and the

Oyashio Extension on the atmospheric circulation. *J. Climate,* **24,** 762–777.

Gershunov, A., and T. P. Barnett, 1998: Interdecadal modulation of ENSO teleconnections. *Bull. Amer. Meteor. Soc.,* **79,** 2715–2725.

Goodrich, G. B., 2007: Influence of the Pacific decadal oscillation on winter precipitation and drought during years of neutral ENSO in the western United States. *Wea. Forecasting,* **22,** 116–124.

Hasselmann, K., 1976: Stochastic climate models, Part 1: Theory. *Tellus,* **28,** 473–485.

Horel, J. D., and J. M. Wallace, 1981: Planetary-scale atmospheric phenomena associated with the Southern Oscillation. *Mon. Wea. Rev.,* **109,** 813–829.

Hu, Z.-Z., and B. Huang, 2009: Interferential impact of ENSO and PDO on dry and wet conditions in the U.S. Great Plains. *J. Climate,* **22,** 6047–6065.

Jha, B., and A. Kumar, 2009: A comparison of the atmospheric response to ENSO in coupled and uncoupled model simulations. *Mon. Wea. Rev.,* **137,** 479–487.

Kumar, A., and M. P. Hoerling, 2000: Analysis of a conceptual model of seasonal climate variability and implications for seasonal predictions. *Bull. Amer. Meteor. Soc.,* **81,** 255–264.

——, ——, M. Ji, A. Leetmaa, and P. Sardeshmukh, 1996: Assessing a GCM's suitability for making seasonal predictions. *J. Climate,* **9,** 115–129.

——, Q. Zhang, J.-K. E. Schemm, M. L' Heureux, and K.-H. Seo, 2008: An assessment of errors in the simulation of atmospheric interannual variability in uncoupled AGCM simulations. *J. Climate,* **21,** 2204–2217.

Kwon, Y.-O., M. A. Alexander, N. A. Bond, C. Frankignoul, H. Nakamura, B. Qiu, and L. Thompson, 2010: Role of the Gulf Stream and Kuroshio–Oyashio systems in large-scale atmosphere–ocean interaction: A review. *J. Climate,* **23,** 3249–3281.

Lau, N.-C., and M. J. Nath, 1996: The role of the ''atmospheric bridge'' in linking tropical Pacific ENSO events to extratropical SST anomalies. *J. Climate,* **9,** 2036–2057.

Liu, Z., 2011: Dynamics of interdecadal climate variability: An historical perspective. *J. Climate,* **25,** 1963–1995.

Mantua, N. J., S. R. Hare, Y. Zhang, J. M. Wallace, and R. Francis, 1997: A Pacific interdecadal climate oscillation with impacts on salmon production. *Bull. Amer. Meteor. Soc.,* **78,** 1069–1079.

Newman, M., G. P. Compo, and M. A. Alexander, 2003: ENSO-forced variability of the Pacific decadal oscillation. *J. Climate,* **16,** 3853–3857.

Pierce, D. W., 2002: The role of sea surface temperatures in interactions between ENSO and the North Pacific Oscillation. *J. Climate,* **15,** 1295–1308.

——, T. P. Barnett, N. Schneider, R. Saravanan, D. Dommenget, and M. Latif, 2001: The role of ocean dynamics in producing decadal climate variability in the North Pacific. *Climate Dyn.,* **18,** 51–70.

Reynolds, R. W., N. A. Rayner, T. M. Smith, D. C. Stokes, and W. Wang, 2002: An improved in situ and satellite SST analysis for climate. *J. Climate,* **15,** 1609–1625.

Robinson, W. A., 2000: Review of WETS—The workshop on extra-tropical SST anomalies. *Bull. Amer. Meteor. Soc.,* **81,** 567–577.

Roy, S. S., G. B. Goodrich, and R. C. Balling Jr., 2003: Influence of El Niño/Southern Oscillation, Pacific decadal oscillation, and local sea surface temperature anomalies on peak season monsoon precipitation in India. *Climate Res.,* **25,** 171–178.

Saha, S., and Coauthors, 2006: The NCEP Climate Forecast System. *J. Climate,* **19,** 3483–3517.

Trenberth, K. E., G. W. Branstator, D. J. Karoly, A. Kumar, N. C. Lau, and C. Ropelewski, 1998: Process during TOGA in understanding and modeling global teleconnections associated with tropical sea surface temperatures. *J. Geophys. Res.,* **103** (C7), 14 291–14 324.

Wang, H., A. Kumar, W. Wang, and Y. Xue, 2012: Influence of ENSO on Pacific decadal variability: An analysis based on the NCEP Climate Forecast System. *J. Climate,* **25,** 6136–6151.

Zhang, Q., A. Kumar, Y. Xue, W. Wang, and F.-F. Jin, 2007: Analysis of the ENSO cycle in the NCEP coupled forecast model. *J. Climate,* **20,** 1265–1284.